CrystEngComm

Accepted Manuscript

ROYAL SOCIETY OF CHEMISTRY

www.rsc.org/crystengcomm

Exploring biphenyl-2,4,4′-tricarboxylic acid as a flexible building block for the hydrothermal self-assembly of diverse metal-organic and supramolecular networks†

Yong-Liang Shao,[a] Yan-Hui Cui,[a] Jin-Zhong Gu,*[a] Jiang Wu,[a] Ya-Wen Wang,*[a] Alexander M. Kirillov[b]

Received (in XXX, XXX) Xth XXXXXXXXX 200X, Accepted Xth XXXXXXXXX 200X
First published on the web Xth XXXXXXXXX 200X
DOI: 10.1039/b000000x

Biphenyl-2,4,4′-tricarboxylic acid (H_3btc) was applied as a principal but still little explored building block for the synthesis of nine new coordination compounds, namely $[Zn(H_2btc)(phen)_2][H_2btc]\cdot H_2O$ (**1**), $[M(H_2btc)_2(H_2biim)_2]$ {M = Co (**2**) and Cd (**3**)}, $[Ni(Hbtc)(phen)_2(H_2O)]\cdot 2H_2O$ (**4**), $[Cd_2(\mu_4\text{-btc})(\mu_2\text{-Cl})(phen)_2]_n$ (**5**), $[Ni_3(\mu_4\text{-btc})_2(\mu_2\text{-}H_2O)_2(py)_4(H_2O)_2]_n$ (**6**), $\{[Co_3(\mu_4\text{-btc})_2(\mu_2\text{-}H_2O)_2(py)_4(H_2O)_2]\cdot(py)_2\}_n$ (**7**), $\{[Co_{3.5}(\mu_6\text{-btc})_2(\mu_3\text{-}OH)(py)_2(H_2O)_3]\cdot H_2O\}_n$ (**8**), and $\{[Pb_3(\mu_6\text{-btc})_2(H_2O)]\cdot H_2O\}_n$ (**9**). These products were easily generated by hydrothermal self-assembly method from the corresponding metal(II) chlorides, H_3btc, and various *N*-donor ancillary ligands, selected from 1,10-phenanthroline (phen), 2,2′-biimidazole (H_2biim), or pyridine (py). The compounds **1**–**9** were characterized by IR spectroscopy, elemental, thermogravimetric, and single-crystal X-ray diffraction analyses. Their structures range from the intricate 3D metal-organic frameworks (MOFs) **6**–**9** to the 2D coordination polymer **5**, and the discrete 0D monomers **1**–**4**. Such a structural diversity is guided by the type of metal(II) node, level of the deprotonation of biphenyl-2,4,4′-tricarboxylic acid, and kind of ancillary ligand. The structures of **1**–**4** are further extended [0D→2D (**1**) and 0D→3D (**2**–**4**)] into various H-bonded networks. Both the supramolecular (in **1**–**4**) and coordination (in **5**–**9**) underlying networks were classified from the topological viewpoint, disclosing the distinct **4,5L64** (in **1**), **pcu** (in **2** and **3**), **sxb** (in **4**), **hcb** (in **5**), and **wei** (in **6** and **7**) topological nets, whereas topologically unique frameworks were identified in MOFs **8** and **9**. The magnetic (for **6**–**8**) and luminescent (for **1**, **3**, **5**, and **9**) properties were also studied and discussed.

Introduction

The design of new coordination polymers and related materials has become a very important research direction spreading between the fields of coordination and inorganic chemistry, crystal engineering and materials chemistry.[1–6] One of the research directions consists of the search for versatile and stable organic building blocks that can be applicable for the facile self-assembly generation of coordination polymers and metal-organic networks based on different metal nodes.[7]

In particular, various biphenyl polycarboxylic acids are well recognized building blocks toward the construction of coordination compounds that possess high-dimensional networks and interesting functional properties, not only due to an ability of such building blocks to adapt a huge diversity of coordination modes and show good thermal stability, but also because of their potential function as H-bond donors and acceptors.[8–11] However, the application of biphenyl polycarboxylate blocks for the generation of metal-organic networks by different self-assembly protocols can be influenced by diverse factors. These include the nature of metal nodes and biphenyl polycarboxylate ligands, presence of templates and ancillary ligands, type of reaction medium, stoichiometry and other reaction conditions.[8a,8b,12–14] Along with biphenyl polycarboxylate building blocks, the introduction into a self-assembly system of aromatic *N*-donor ancillary ligands (possessing effective π···π stacking and/or weak H-bonding interactions) has also often been used to facilitate crystallization and stabilize new structures.[8a-c,15–18]

Aiming at the synthesis of novel metal-organic networks and following our interest in this field,[2a,8a-c,19,20] we have selected biphenyl-2,4,4′-tricarboxylic acid (H_3btc) as a principal building block and tested it in the hydrothermal self-assembly reactions with different metal(II) nitrates (M = Zn, Cd, Co, Ni, Pb), and in the presence of 1,10-phenanthroline (phen), 2,2′-biimidazole (H_2biim), or pyridine (py) as aromatic *N*-donor ancillary ligands. The selection of H_3btc was governed not only due to the presence of three carboxylic groups that can exhibit a different degree of deprotonation and thus diverse coordination modes, but also owing to the flexibility of biphenyl core wherein the aromatic rings can rotate around the C–C single bond. Besides, although several coordination polymers derived from H_3btc have been reported,[8b,c] this carboxylic acid block still remains little explored in the crystal engineering of coordination polymers and related derivatives.

Hence, in the present work we report the hydrothermal self-assembly generation, characterization, thermal stability, structural and topological features, and luminescent or magnetic properties of a new series of nine coordination compounds derived from H_3btc and various *N*-donor ancillary ligands, namely 3D metal-organic frameworks $[Ni_3(\mu_4\text{-btc})_2(py)_4(\mu_2\text{-}H_2O)_2(H_2O)_2]_n$ (**6**), $\{[Co_3(\mu_4\text{-btc})_2(\mu_2\text{-}H_2O)_2(py)_4(H_2O)_2]\cdot(py)_2\}_n$ (**7**), $\{[Co_{3.5}(\mu_6\text{-btc})_2(\mu_3\text{-}OH)(py)_2(H_2O)_3]\cdot H_2O\}_n$ (**8**), and $\{[Pb_3(\mu_6\text{-btc})_2(H_2O)]\cdot H_2O\}_n$ (**9**), 2D coordination polymer $[Cd_2(\mu_4\text{-btc})(\mu_2\text{-}Cl)(phen)_2]_n$ (**5**), and discrete 0D complexes $[Zn(H_2btc)(phen)_2][H_2btc]\cdot H_2O$ (**1**), $[M(H_2btc)_2(H_2biim)_2]$ {M = Co (**2**) and Cd (**3**)}, $[Ni(Hbtc)(phen)_2(H_2O)]\cdot 2H_2O$ (**4**). Their diversity proves that the nature of metal node and ancillary ligand has an important effect on the generation and structural and topological characteristics of the final products **1**–**9**. Apart from structural and topological novelties, an important feature of the obtained products consists in their facile self-assembly preparation using water as a medium of crystallization. This constrasts with common crystal engineering synthetic procedures for metal-organic networks that typically require the use of an organic solvent.[1–7]

Experimental section

Materials and methods

All chemicals and solvents were of A.R. grade and used without further purification. Carbon, hydrogen and nitrogen were determined using an Elementar Vario EL elemental analyzer. IR spectra were recorded using KBr pellets and a Bruker EQUINOX 55 spectrometer. Melting points were measured in air on XT-4 melting point detector. Thermogravimetric analysis (TGA) was performed under N_2 atmosphere with a heating rate of 10 °C/min on a LINSEIS STA PT1600 thermal analyzer. Powder X-ray diffraction patterns (PXRD) were determined with a Rigaku-Dmax 2400 diffractometer using Cu-*K*α radiation (λ = 1.54060 Å), in which the X-ray tube was operated at 40 kV and 40 mV. Magnetic susceptibility data were collected in the 2–300 K temperature range with a Quantum Design SQUID Magnetometer MPMS XL-7 with a field of 0.1 T. A correction was made for the diamagnetic contribution prior to data analysis. Excitation and emission spectra were recorded for the solid samples on an Edinburgh FLS920 fluorescence spectrometer at room temperature.

Synthesis of $[Zn(H_2btc)(phen)_2][H_2btc]\cdot H_2O$ (1). A mixture of $ZnCl_2$ (40.9 mg, 0.15 mmol), H_3btc (85.9 mg, 0.3 mmol), phen (60.0 mg, 0.30 mmol), NaOH (12.0 mg, 0.3 mmol), and H_2O (10 mL) was stirred at room temperature for 15 min, then sealed in a 25 mL Teflon-lined stainless steel vessel, and heated at 160 °C for 3 days, followed by cooling to room temperature at a rate of 10 °C/h. Coloureless block-shaped crystals were isolated manually, washed with distilled water and dried to give **1**. Yield: 65% (based on H_3btc). Calcd for $C_{54}H_{36}ZnN_4O_{13}$: C 63.94, H 3.58, N 5.52%. Found: C 64.21, H 3.53, N 5.48%; mp = 332 °C (dec.). IR (KBr, cm^{-1}): 3392 w, 3060 w, 1726 m, 1612 s, 1582 w, 1542 w, 1514 w, 1428 s, 1394 w, 1370 w, 1348 m, 1244 w, 1226 w, 1180 w, 1146 w, 1106 w, 1054 w, 1008 w, 928 w, 848 s, 824 w, 784 m, 728 s, 670 w, 646 w, 566 w, 526 w.

Synthesis of $[M(H_2btc)_2(H_2biim)_2]$ (M = Co (2) and Cd (3)). A mixture of $MCl_2\cdot xH_2O$ (x = 6 for **2** and x = 1 for **3**, 0.15 mmol), H_3btc (85.9 mg, 0.3 mmol), H_2biim (40.2 mg, 0.30 mmol), NaOH (12.0 mg, 0.3 mmol), and H_2O (10 mL) was stirred at room temperature for 15 min, then sealed in a 25 mL Teflon-lined stainless steel vessel, and heated at 160 °C for 3 days, followed by cooling to room temperature at a rate of 10 °C/h. Yellow or colorless crystals were isolated manually, washed with distilled water and dried to furnish compounds **2** and **3**, respectively. Yield: 50% for **2**, 55% for **3** (based on H_3btc). Calcd for $C_{42}H_{30}CoN_8O_{12}$ (**2**): C 56.20, H 3.37, N

12.48%. Found: C 56.11, H 3.41, N 12.40%; mp = 238 °C (dec.). IR (KBr, cm^{-1}): 1686 s, 1587 s, 1552 w, 1425 w, 1384 s, 1320 w, 1290 m, 1184 w, 1159 w, 1124 m, 992 m, 929 w, 879 w, 858 w, 810 w, 787 w, 765 s, 692 m, 679 w, 606 w, 542 w. Calcd for $C_{42}H_{30}CdN_8O_{12}$ (**3**): C 53.04, H 3.18, N 11.78%.

Synthesis of [Ni(Hbtc)(phen)$_2$(H$_2$O)]·2H$_2$O (4). A mixture of $NiCl_2{\cdot}6H_2O$ (71.1 mg, 0.30 mmol), H_3btc (85.9 mg, 0.3 mmol), phen (120.0 mg, 0.60 mmol), NaOH (24.0 mg, 0.60 mmol), and H_2O (10 mL) was stirred at room temperature for 15 min, then sealed in a 25 mL Teflon-lined stainless steel vessel, and heated at 160 °C for 3 days, followed by cooling to room temperature at a rate of 10 °C/h. Purple needle-shaped crystals were isolated manually, washed with distilled water and dried to produce **4**. Yield: 60% (based on H_3btc). Calcd for $C_{39}H_{30}NiN_4O_9$: C 61.85, H 3.99, N 7.40%. Found: C 61.95, H 3.95, N 7.51%; mp = 286 °C (dec.). IR (KBr, cm^{-1}): 3450 m, 3064 w, 1686 w, 1626 s, 1604 s, 1584 m, 1547 s, 1516 m, 1424 s, 1369 s, 1343 w, 1223 w, 1141 w, 1104 w, 1051 w, 907 w, 869 w, 845 s, 807 w, 788 w, 772 m, 727 s, 710 w, 684 m, 662 w, 644 w, 552 w.

Synthesis of [Cd$_2$(μ$_4$-btc)(μ$_2$-Cl)(phen)$_2$]$_n$ (5). A mixture of $CdCl_2{\cdot}H_2O$ (90.6 mg, 0.45 mmol), H_3btc (85.9 mg, 0.3 mmol), phen (90.0 mg, 0.45 mmol), NaOH (36.0 mg, 0.9 mmol), and H_2O (10 mL) was stirred at room temperature for 15 min, then sealed in a 25 mL Teflon-lined stainless steel vessel, and heated at 160 °C for 3 days, followed by cooling to room temperature at a rate of 10 °C/h. Colorless block-shaped crystals were isolated manually, washed with distilled water and dried to give **5**. Yield: 60% (based on H_3btc). Calcd for $C_{39}H_{23}ClCd_2N_4O_6$: C 51.82, H 2.56, N 6.20%. Found: C 51.71, H 2.58, N 6.13%; mp = 303 °C (dec.). IR (KBr, cm^{-1}): 1575 s, 1542 s, 1517 s, 1426 s, 1396 s, 1343 w, 1254 w, 1222 w, 1168 w, 1143 w, 1102 m, 1050 w, 1027 w, 1005 w, 969 w, 925 w, 880 w, 860 m, 847 s, 832 m, 798 w, 783 s, 725 s, 700 m, 664 w, 638 w, 546 w.

Synthesis of [Ni$_3$(μ$_4$-btc)$_2$(py)$_4$(μ$_2$-H$_2$O)$_2$(H$_2$O)$_2$]$_n$ (6). A mixture of $NiCl_2{\cdot}6H_2O$ (107.0 mg, 0.45 mmol), H_3btc (85.9 mg, 0.3 mmol), py (0.5 mL, 6.3 mmol), and H_2O (10 mL) was stirred at room temperature for 15 min, then sealed in a 25 mL Teflon-lined stainless steel vessel, and heated at 160 °C for 3 days, followed by cooling to room temperature at a rate of 10 °C/h. Green block-shaped crystals were isolated manually, washed with distilled water and dried to produce **6**. Yield: 65% (based on H_3btc). Calcd for $C_{49}H_{42}Ni_3N_4O_{16}$: C 52.60, H 3.78, N 5.01%. Found: C 52.68, H 3.72, N 5.7%; mp = 135 °C (dec.). IR (KBr, cm^{-1}): 3332 m, 1605 s, 1547 m, 1488 w, 1446 m, 1382 s, 1244 w, 1220 w, 1152 w, 1072 w, 1042 w, 1005 w, 938 w, 875 w, 858 w, 836 w, 814 w, 797 w, 781 m, 758 w, 697 s, 666 w, 631 w, 561 w.

Synthesis of {[Co$_3$(μ$_4$-btc)$_2$(μ$_2$-H$_2$O)$_2$(py)$_4$(H$_2$O)$_2$]·(py)$_2$}$_n$ (7). The preparation of **7** was similar to that of **6** except using $CoCl_2{\cdot}6H_2O$ instead of $NiCl_2{\cdot}6H_2O$. After cooling the reaction mixture to room temperature, pink block-shaped crystals were isolated manually, washed with distilled water and dried to give **7**. Yield: 50% (based on H_3btc). Calcd for $C_{60}H_{52}Co_3N_6O_{16}$: C 55.87, H 4.06, N 6.52%. Found: C 55.73, H 4.09, N 6.62%; mp = 122 °C (dec.). IR (KBr, cm^{-1}): 3386 m, 1603 s, 1546 m, 1488 w, 1446 m, 1383 s, 1245 w, 1220 w, Found: C 52.91, H 3.21, N 11.85%; mp = 275 °C (dec.). IR (KBr, cm^{-1}): 1686 m, 1606 s, 1554 s, 1428 s, 1376 s, 1312 w, 1290 w, 1256 w, 1180 w, 1124 w, 1094 w, 992 w, 940 w, 854 w, 824 w, 790 m, 756 m, 710 w, 682 w, 560 w, 520 w, 480 w, 428 w.

1179 w, 1152 w, 1136 w, 1100 w, 1072 w, 1041 w, 1006 w, 938 w, 875 w, 857 w, 833 w, 781 m, 757 w, 699 m, 690 m, 665 w, 629 w, 557 w.

Synthesis of {[Co$_{3.5}$(μ$_6$-btc)$_2$(μ$_3$-OH)(py)$_2$(H$_2$O)$_3$]·H$_2$O}$_n$ (8). The preparation of **8** was similar to that of **7** except using different amout of $CoCl_2{\cdot}6H_2O$ (126.0 mg, 0.53 mmol). After cooling the reaction mixture room temperature, pink block-shaped crystals were isolated manually, washed with distilled water and dried to furnish **8**. Yield: 55% (based on H_3btc). Calcd for $C_{40}H_{33}Co_{3.5}N_2O_{17}$: C 47.10, H 3.26, N 2.75%. Found: C 47.25, H 3.22, N 2.72%; mp = 80 °C (dec.). IR (KBr, cm^{-1}): 3437 m, 1637 m, 1603 s, 1582 m, 1536 m, 1487 w, 1448 w, 1382 s, 1242 w, 1218 w, 1177 w, 1154 w, 1130 w, 1096 w, 1071 w, 1004 w, 942 w, 877 w, 841 w, 778 m, 756 w, 724 w, 696 m, 665 w, 634 w, 534 w.

Synthesis of {[Pb$_3$(μ$_6$-btc)$_2$(H$_2$O)]·H$_2$O}$_n$ (9). A mixture of $PbCl_2$ (125.1 mg, 0.45 mmol), H_3btc (85.9 mg, 0.3 mmol), NaOH (36.0 mg, 0.9 mmol), and H_2O (10 mL) was stirred at room temperature for 15 min, then sealed in a 25 mL Teflon-lined stainless steel vessel, and heated at 160 °C for 3 days, followed by cooling to room temperature at a rate of 10 °C/h. Colorless block-shaped crystals were isolated manually, washed with distilled water and dried to produce **9**. Yield: 65% (based on H_3btc). Calcd for $C_{30}H_{18}Pb_3O_{14}$: C 29.44, H 1.48%. Found: C 29.38, H 1.45%; mp = 371 °C (dec.). IR (KBr, cm^{-1}): 3416 m, 1606 s, 1578 s, 1520 s, 1434 w, 1376 s, 1250 w, 1180 w, 1130 w, 1100 w, 1054 w, 1002 w, 952 w, 928 w, 882 w, 854 w, 824 w, 784 m, 738 w, 716 w, 686 m, 658 w, 578 w, 526 w.

X-ray data collection and structure determination

The X-ray single-crystal data collection for **1–9** was performed on a Bruker Smart CCD or an Agilent SuperNova diffractometers, using graphite-monochromated Mo K_α radiation (λ = 0.71073 Å). Semiempirical absorption corrections were applied using the SADABS program. The structures were solved by direct methods and refined by full-matrix least-squares on F^2 using the SHELXS-97 and SHELXL-97 programs.[21] All the non-hydrogen atoms were refined anisotropically by full-matrix least-squares methods on F^2. All the hydrogen atoms (except the those bound to water molecules) were placed in calculated positions with fixed isotropic thermal parameters and included in structure factor calculations in the final stage of full-matrix least-squares refinement. The hydrogen atoms of water molecules were located by difference maps and constrained to ride on their parent O atoms. In compound **6**, four pyridine C atoms are disordered over two sites, that is, C21A, C22A, C24A, C25A and C21B, C22B, C24B, C25B, with occupancy of 0.5. In compound **7**, four pyridine C atoms are disordered over two sites, that is, C26, C27, C29, C30 and C26’, C27’, C29’, C30’, with occupancy of 0.5. The details of the crystal parameters, data collections and refinement for **1–9** are summarized in Table 1 and the selected bond lengths are listed in Table S1 (ESI†). Hydrogen bonds for the compounds **1**–**4** and **6**–**9** are given in Table S2 (ESI†). The topological analysis of the H-bonded networks in **1**–**4** was carried out taking into consideration only the conventional (strong) hydrogen bonds D–H···A, wherein H···A <2.50 Å, D···A <3.50 Å, ∠(D–H···A) >120°, D and A stand for donor and acceptor atoms.[22] For the topological analysis of H-bonded (**1**–**4**) and metal-organic (**5**–**9**) networks, the concept of the the simplified underlying net was followed.[22] CCDC-1430225–1430233 for **1**–**9** contain the supplementary crystallographic data for this paper.

Table 1 Crystallographic data and structure refinement summary for **1**–**9**

Compound	**1**	**2**	**3**	**4**	**5**	**6**	**7**	**8**	**9**
Chemical formula	$C_{54}H_{36}ZnN_4O_{13}$	$C_{42}H_{30}CoN_8O_{12}$	$C_{42}H_{30}CdN_8O_{12}$	$C_{39}H_{30}Ni\ N_4O_9$	$C_{39}H_{23}Cd_2ClN_4O_6$	$C_{49}H_{42}Ni_3N_4O_{16}$	$C_{60}H_{52}Co_3N_6O_{16}$	$C_{40}H_{33}Co_{3.5}N_2O_{17}$	$C_{30}H_{18}Pb_3O_{14}$
Formula weight	1014.24	897.67	951.14	757.38	903.86	1289.86	1289.86	1019.94	1224.01
Crystal system	Triclinic	Triclinic	Triclinic	Orthorhombic	Orthorhombic	Monoclinic	Monoclinic	Triclinic	Monoclinic
Space group	*P*-1	*P*-1	*P*-1	*P*na2$_1$	*P*ca2$_1$	*C*2/c	*C*2/c	*P*-1	*P*2$_1$/n
a/Å	11.8801(11)	8.0674(10)	8.0767(4)	14.3366(12)	20.3729(6)	20.505(2)	20.600(5)	12.0580(7)	13.48481(14)
b/Å	13.7323(17)	9.2640(15)	9.4789(8)	13.9193(7)	9.7388(3)	10.3482(9)	10.4271(11)	12.3182(6)	12.16380(14)
c/Å	13.9872(19)	13.4563(18)	13.3988(11)	17.1433(9)	17.7787(6)	29.521(4)	29.646(5)	15.3976(8)	17.6457(2)
α/°	84.567(11)	72.758(13)	73.886(7)	90	90	90	90	67.945(5)	90
β/°	79.104(9)	83.095(11)	83.844(5)	90	90	113.518(15)	113.51(2)	88.887(4)	95.1954(10)
γ/°	79.225(9)	82.579(12)	80.810(6)	90	90	90	90	80.778(4)	90
V/Å^3	2197.1(5)	948.9(2)	970.70(12)	3421.0(4)	3527.44(19)	5743.7(13)	5840(2)	2090.23(19)	2882.46(6)
T/K	293(2)	293(2)	293(2)	293(2)	293(2)	293(2)	293(2)	293(2)	293(2)
Z	2	1	1	4	4	4	4	2	4
D_c/g cm^{-3}	1.533	1.571	1.627	1.470	1.702	1.294	1.467	1.621	2.821
μ/mm^{-1}	0.638	0.533	0.642	0.632	1.335	1.038	0.917	1.446	34.188
F(000)	1044	461	482	1568	1784	2304	2652	1035	2224
Refl. measured	16042	5859	6260	7827	14089	12802	10401	12260	11000
Unique refl. (R_{int})	7782 (0.1017)	3360 (0.0485)	3446(0.0563)	5279 (0.0648)	5698 (0.0595)	5648 (0.1081)	5169 (0.1043)	7125 (0.0638)	5347 (0.0360)
GOF on F^2	1.015	1.032	1.061	1.010	1.042	0.933	1.041	1.022	0.965
R_1 $[I > 2\sigma(I)]^a$	0.0770	0.0791	0.0597	0.0699	0.0515	0.0873	0.0829	0.0704	0.0287
wR_2 $[I > 2\sigma(I)]^b$	0.1251	0.1877	0.1188	0.1223	0.1234	0.1803	0.1680	0.1741	0.0493

^{a} $R_1 = \Sigma||F_o| - |F_c||/|F_o|$. ^{b} $wR_2 = \{\Sigma[w(F_o^2 - F_c^2)]^2/\Sigma[w(F_o^2)]^2\}^{1/2}$.

Results and discussion

Crystal structure of 1. Compound **1** crystallizes in the triclinic space group *P*–1 and its asymmetric unit contains one $[Zn(H_2btc)(phen)_2]^+$ cation, one H_2btc^- anion, and one lattice water molecule (Fig. 1a). In the cation, Zn(II) atom adopts a distorted octahedral $\{ZnN_4O_2\}$ geometry formed by two carboxylate O atoms of H_2btc^- ligand and four N atoms of two phen moieties. The Zn–O bonds range from 2.172(4) to 2.260(4) Å, whereas the Zn–N distances vary from 2.096(5) to 2.156(5) Å, which are comparable to those found in other reported Zn(II) compounds.[3b,3d,6a,6b,18,20] The H_2btc^- moiety acts as a terminal ligand (Scheme 1, mode I) with a deprotonated carboxylate group showing a η^1:η^1 bidentate mode. The dihedral angles between two phenyl rings in the H_2btc^- ligand and anion are 39.51 and 60.16°, respectively. The discrete units of **1** are interlinked by the strong O–H···O hydrogen bonds involving H_2btc^- anions and water molecules of crystallization, forming a 2D supramolecular network (Fig. 1b, Table 3). From the topological viewpoint, this network can be described as a binodal 4,5-connected layer with the **4,5L64** topology (Fig. 1c). It is defined by the point symbol of $(4^4.6^2)(4^6.6^4)$, wherein the $(4^4.6^2)$ and $(4^6.6^4)$ notations are those of the H_2btc^- anions and $[Zn(H_2btc)(phen)_2]^+$ nodes, respectively.

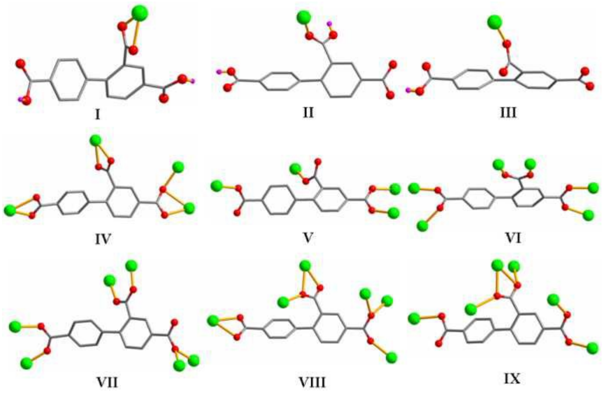

Scheme 1 Various coordination modes of H_2btc^- / $Hbtc^{2-}$ / btc^{3-} in compounds **1**–**9**.

Crystal structure of 2. Single-crystal X-ray analyses reveal that compounds **2** and **3** are isostructural; the structure of **2** is described in detail as a representative example (Fig. 2). The discrete 0D monomer **2** crystallizes in the triclinic space group *P*–1 and its asymmetric unit contains one Co(II) atom, two H_2L^- ligands, and two H_2biim moieties. As shown in Fig. 2a, the six-coordinate Co(II) center is bound by a pair of O atoms from two monodentate H_2L^- ligands and four N atoms from two chelating H_2biim moieties, thus forming an ideal octahedral $\{CoN_4O_2\}$ geometry. The Co–O bonds are

2.210(4) Å, while the Co–N distances vary from 2.126(5) to 2.129(5) Å; all these distances are comparable to those found in the reported Co(II) compounds.[2b,3d,4a,8a] In **2**, the H_2L^- acts as a terminal ligand (Scheme 1, mode II), in which the carboxylate group is in the η^1:η^0 monodentate mode. The dihedral angle between the two phenyl rings in the H_2L^- block is 43.73°. The discrete monomeric units of **2** are interlinked by the strong O–H···O and N–H···O hydrogen bonds to form a 3D supramolecular framework (Fig. 2b, Table 2). From the topological viewpoint, this 3D H-bonded net can be classified as a uninodal 6-connected framework with the **pcu** [alpha-Po primitive cubic] topology and point symbol of $(4^{12}.6^3)$ (Fig. 2c).

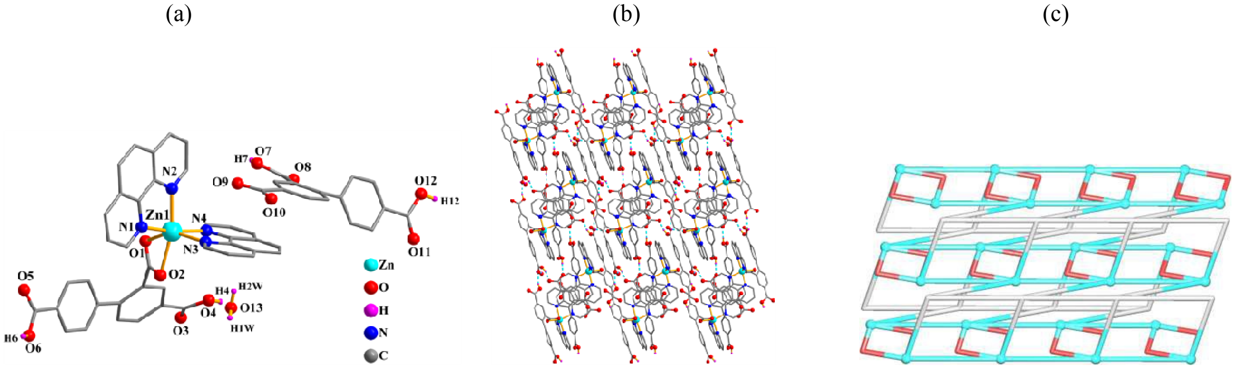

Fig. 1 Structural fragments of **1**. (a) Coordination environment of the Zn(II) atom. (b) Perspective of the 2D supramolecular network along the *ac* plane. (c) Topological representation of the underlying 2D H-bonded network showing a binodal 4,5-connected layer with the **4,5L64** topology; view along the *b* axis; color codes: centroids of 5-connected $[Zn(H_2btc)(phen)_2]^+$ cations (cyan balls), centroids of 4-connected H_2btc^- anions (gray), centroids of H_2O linkers (red).

Crystal structure of 4. The compound **4** crystallizes in the orthorhombic space group $Pna2_1$ and also features a discrete 0D monomer structure. The asymmetric unit bears one Ni(II) atom, one terminal $Hbtc^{2-}$ and two phen ligands, one coordinated and two lattice water molecules. As depicted in Fig. 3a, the six-coordinate Ni(II) atom adopts a distorted octahedral $\{NiN_4O_2\}$ geometry taken by one carboxylate O atom from $Hbtc^{2-}$ block, one O atom from H_2O ligand, and four N atoms from two phen moieties. The Ni–O and Ni–N bond distances are in the 2.061(8)–2.073(7) and 2.084(9)–2.107(10) Å ranges, respectively; these are within the normal values observed in related Ni(II) coordination compounds.[1l,2b,3d,6a] In **4**, the $Hbtc^{2-}$ moiety acts as terminal ligand, with the 2-carboxylate group adopting a η^1:η^0 monodentate mode (Scheme 1, mode The dihedral angle between the two phenyl rings in the HL^{2-} block is 56.64°. The discrete mononickel(II) units and lattice water molecules are held together by the strong O–H···O hydrogen bonds to generate a 3D supramolecular framework (Fig. 3b, Table 2). This framework can be topologically classified as a uninodal 6-connected underlying net (Fig. 3c) with the **sxb** topology and point symbol of $(4^8.5^4.6^3)$.[22]

Crystal structure of 5. The asymmetric unit of **5** consists of two crystallographically independent Cd(II) atoms, one μ_4-btc^{3-} block, one μ_2-Cl ligand, and two phen moieties. As depicted in Fig. 4a, both the six-coordinate Cd1 and Cd2 atoms possess a distorted octahedral $\{CdClN_2O_3\}$ environment. The Cd1 and Cd2 centers are surrounded by three O atoms from two different μ_4-btc^{3-} blocks, one μ_2-Cl^- ligand, and two N atoms from one phen moiety. The Cd–O, Cd–N, and Cd–Cl bond distances are in the 2.271(6)–2.468(9), 2.331(8)–2.399(9), and 2.543(2)–2.628(3) Å ranges, respectively; these are within the normal values observed in various Cd(II) coordination compounds.[6a,8a,10b,20,23]

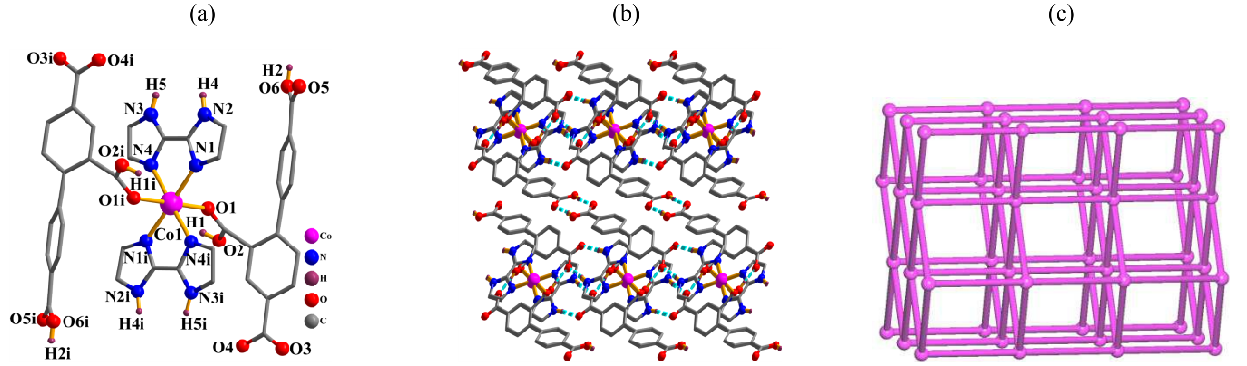

Fig. 2 Structural fragments of **2**. (a) Coordination environment of the Co(II) atom. Symmetry code: i = –*x*+1, –*y*+2, –*z*. (b) 3D H-bonded framework along the *ac* plane (blue dashed lines represent the H-bonds). (c) Topological representation of the underlying 3D H-bonded network showing a uninodal 6-connected net with the **pcu** topology; view along the *a* axis; color code: centroids of 6-connected $[Co(H_2btc)_2(H_2bimz)_2]$ molecular nodes (magenta balls).

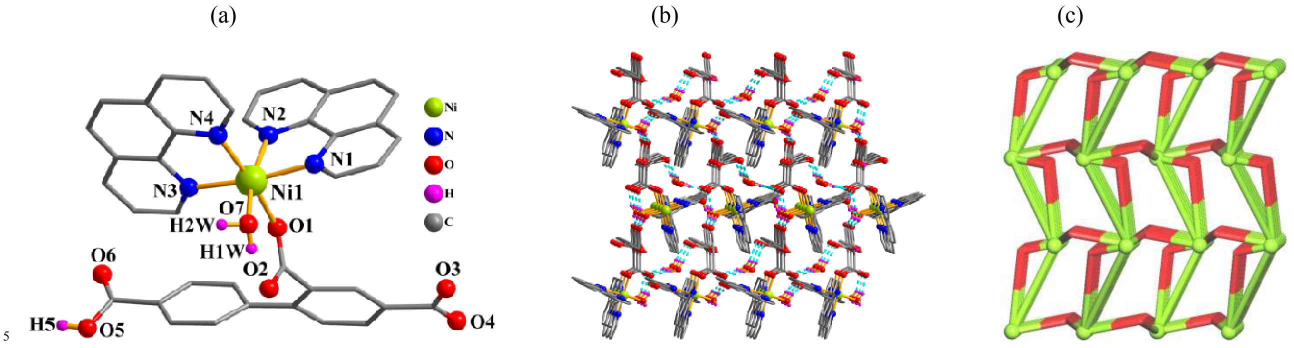

Fig. 3 Structural fragments of **4**. (a) Coordination environment of the Ni(II) atom. (b) Perspective of a 3D supramolecular framework along the *ac* plane (blue lines present the H-bonds). (d) Topological representation of the underlying 3D H-bonded network showing a uninodal 6-connected net with the **sxb** topology; view along the *b* axis; color codes: centroids of 6-connected [Ni(Hbtc)(phen)$_2$(H$_2$O)] molecular nodes (green balls), centroids of H$_2$O linkers (red).

In **5**, the btc^{3-} spacer exhibits a μ_4-coordination mode (Scheme 1, mode IV), in which the three carboxylate groups show different μ_2-η^1:η^1 bidentate or μ_2-η^2:η^1 tridentate modes. The dihedral angle between two phenyl rings in the btc^{3-} is 40.37°. One carboxylate group from μ_4-btc^{3-} block and one μ_2-Cl$^-$ moiety bridge two adjacent Cd(II) atoms to form a dicadmium(II) unit (Fig. 4b) with a Cd···Cd separation of 3.625(3) Å and the Cd–Cl–Cd and Cd–O–Cd angles of 89.02 and 91.97°. Several similar mixed bridged cores were reported.[23] The Cd$_2$ units are further connected by the btc^{3-} ligands to generate a 2D metal-organic layer (Fig. 4b). The 2D sheets are additionally extended into a 3D supramolecular framework by O–H···Cl hydrogen bonds (Fig. S1, ESI†). From the topological viewpoint,[22] the underlying network of **5** (Fig. 4c) can be considered as a uninodal 3-connected layer with the **hcb** [Shubnikov hexagonal plane net/(6,3)] topology and point symbol of (6^3). This layer is composed of the topologically equivalent 3-connected [Cd$_2$(μ_2-Cl)(phen)$_2$]$^{3+}$ and btc^{3-} nodes.

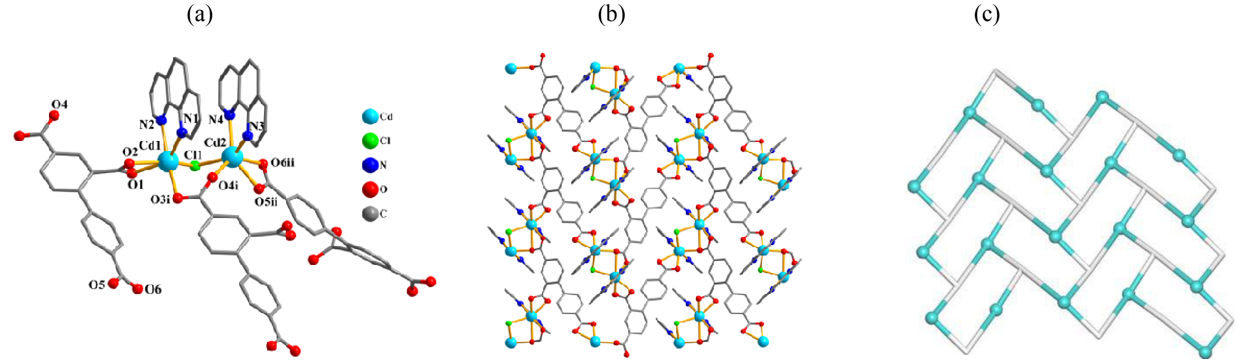

Fig. 4 Structural fragments of **5**. (a) Coordination environment of the Cd(II) atoms. Symmetry codes: i = x, y – 1, z; ii = –x + 1, –y, z + 1/2. (b) Perspective of the 2D metal-organic sheet along the *bc* plane. (c) Topological representation of the underlying 2D network showing a uninodal 3-connected layer with the **hcb** topology; view along the *a* axis; color codes: centroids of 3-connected [Cd$_2$(μ$_2$-Cl)(phen)$_2$]$^{3+}$ (turquoise balls) and btc^{3-} (gray) nodes.

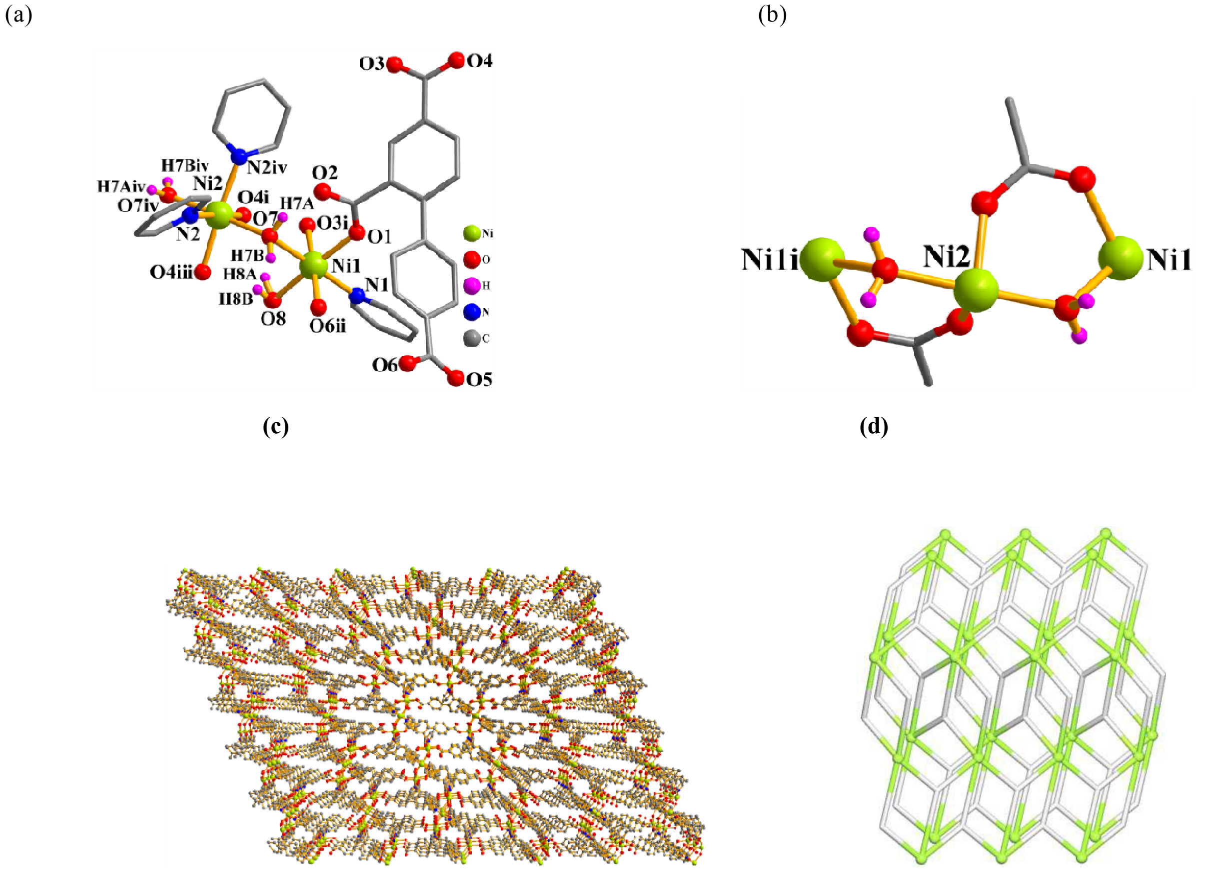
(a) (b)

(c) (d)

Fig. 5 Structural fragments of **6**. (a) Coordination environment of the Ni(II) atoms. Symmetry codes: i = –*x* + 1/2, *y* – 1/2, –*z* + 1/2; ii = –*x* + 1/2, –*y* + 3/2, –*z*; iii = *x* + 1/2, *y* – 1/2, *z*; iv = –*x* + 1, *y*, –*z* + 1/2. (b) Trinuclear Ni(II) subunit. Symmetry code: i = –*x* + 1, *y*, –*z* + 1/2. (c) A perspective of 3D porous metal-organic framework along the *ac* plane. (d) Topological representation of the underlying 3D framework showing a binodal 3,6-connected net with the **ant** (anatase) topology; view along the *b* axis; color codes: centroids of 6-connected $[Ni_3(\mu_2\text{-}H_2O)_2(py)_4(H_2O)_2]^{4+}$ cluster nodes (green balls), centroids of 3-connected btc^{3-} nodes (gray).

Crystal structures of 6 and 7. Single-crystal X-ray diffraction analysis reveals that the compounds **6** and **7** are isostructural and, therefore, only **6** is described in detail as a representative example. The asymmetric unit of **6** consists of two crystallographically distinct nickel(II) atoms (Ni1 with full occupancy and Ni2 with half occupancy), one μ_4-btc^{3-} block, two pyridine and one μ_2-H_2O ligands, and one water molecule of crystallization. As shown in Fig. 5a, the six-coordinate Ni1 atom adopts a distorted $\{NiNO_5\}$ octahedral geometry, filled by three O atoms from the three distinct btc^{3-} blocks, two O atoms from bridging and terminal H_2O ligands, and one N atom of py moiety. The Ni2 atom is located on a 2-fold rotation axis and is coordinated by two O atoms from the two different btc^{3-} blocks, two O atoms from μ_2-H_2O ligands, and two N atoms of two py moieties, thus forming a distorted octahedral $\{NiN_2O_4\}$ geometry. The Ni–O bond lengths range from 2.044(5) to 2.150(4) Å, while the Ni–N distances vary from 2.068(6) to 2.135(5) Å, being comparable to those found in some reported Ni(II) compounds.[2b,3d,8b] In **6**, the btc^{3-} spacer exhibits a μ_4-coordination mode (Scheme 1, mode V), in which the three carboxylate groups adopt different η^1:η^0 monodentate or μ_2-η^1:η^1 bidentate modes. The dihedral angle between two phenyl rings in btc^{3-} is 48.15°. The three adjacent Ni(II) ions are bridged by means of two carboxylate groups from the two different btc^{3-} blocks and two μ_2-H_2O ligands, giving rise to a trinickel(II) subunit (Fig. 5b). In this Ni_3 subunit, the Ni···Ni distance of 3.717(6) Å is longer than those reported for other carboxylate and H_2O-bridged trinuclear Ni(II) cores.[24] The adjacent Ni_3 subunits are multiply interlinked by the btc^{3-} blocks into a 3D metal-organic framework (Fig. 5c), having the shortest distance of 8.922(8) Å between the neighboring trinickel(II) subunits. The framework possesses channels with a dimension of 6.73 × 6.43 Å, measured by atom-to-atom distances. Upon removal of coordinated and lattice water molecules, the PLATON analysis revealed that the network free volume is 11.2% of the crystal volume.[25] From the topological viewpoint, an underlying 3D framework of **6** is assembled from the 4-connected Ni1, Ni2, and μ_4-btc^{3-} nodes, as well as the 2-connected μ_2-H_2O linkers. Topological analysis of this net reveals a binodal 4,4-connected framework with a rare **wei** topology and point symbol of $(3.4.6.7.8^2)_4(3^2.6^2.7^2)$. Although this topological type has been predicted, compound **6** appears to be the first identified example of MOF with the present topology.[22,26–28] Alternative simplification of **6** by considering the $[Ni_3(\mu_2\text{-}H_2O)_2(py)_4(H_2O)_2]^{4+}$ SBUs as the 6-connected cluster nodes can give rise to a binodal 3,6-connected net with the **ant** (anatase) topology (Fig. 5d). It is defined by the point symbol of $(4^2.6)_2(4^4.6^2.8^8.10)$ with the $(4^2.6)$ and $(4^4.6^2.8^8.10)$

notations corresponding to the btc^{3-} and trinickel(II) nodes, respectively.

Crystal structure of 8. The asymmetric unit of **8** contains four crystallographically unique Co(II) ions (three with full occupancy and one with half occupancy), two μ_6-btc^{3-} blocks, one μ_3-OH$^-$ ligand, two py moieties, and three coordinated and one lattice water molecules. As depicted in Fig. 6a, the Co1 atom is six-coordinated by three O atoms of three different btc^{3-} blocks, one O atom from μ_3-OH$^-$ ligand, and two O atoms of coordinated water molecules, constructing a distorted octahedral {CoO$_6$} geometry. The six-coordinate Co2 atom is also surrounded by three carboxylate O atoms of three independent btc^{3-} blocks, one O atom from μ_3-OH$^-$ ligand, one O atom of coordinated water molecule, and one N atom from py moiety, forming a distorted octahedral {CoNO$_5$} geometry. The Co3 atom is located at the inversion site and is coordinated by four O atoms from the four individual btc^{3-} blocks, two O atoms from two μ_3-OH$^-$ ligands, forming an octahedral {CoO$_6$} geometry. The Co4 center possesses a distorted square pyramidal {CoNO$_4$} environment, occupied by four O atoms of four different btc^{3-} blocks and one N atom of py ligand. The lengths of the Co–O bonds range from 1.964(5) to 2.224(6) Å, whereas the Co–N bonds vary from 2.074(6) to 2.110(7) Å; these bonding parameters lie within the typical values observed in various related cobalt(II) derivatives.[3d,4a,8a,8b,11]

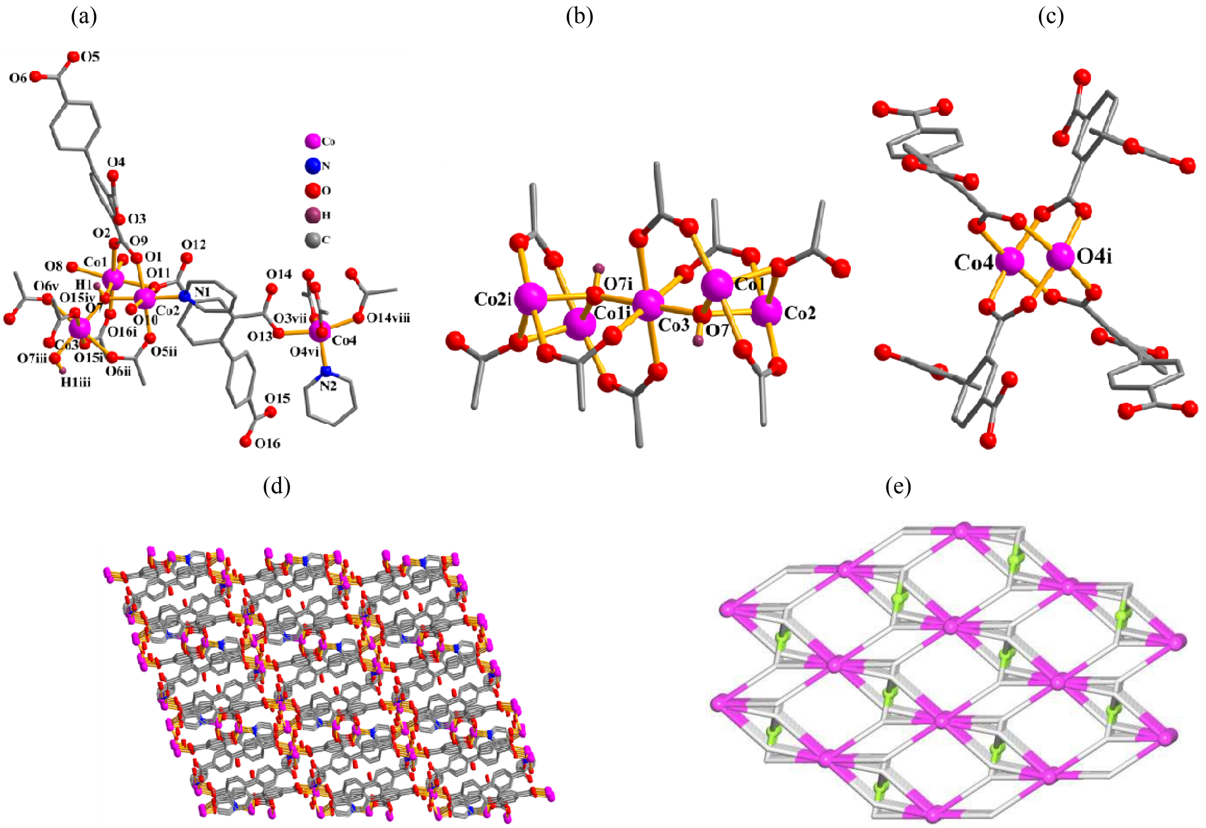

Fig. 6 Structural fragments of **8**. (a) Coordination environment of the Co(II) atoms. Symmetry codes: i = –*x*, –*y* + 1, –*z* + 1; ii = *x*, *y*, *z* + 1; iii = –*x*, –*y* + 2, –*z*; iv = *x*, *y* + 1, *z* – 1; v = –*x*, –*y* + 2, –*z* – 1 ; vi = –*x* + 1, –*y* + 1, –*z*; vii = *x*, *y* – 1, *z* + 1; viii = –*x* + 1, –*y*, –*z* + 1. (b) Pentacobalt(II) subunit. Symmetry codes: i = –*x*, –*y* + 2, –*z*. (c) Dicobalt(II) subunit. Symmetry code: i = –*x* + 1, –*y*, –*z* + 1. (d) A perspective of 3D metal-organic framework along the *bc* plane. (e) Topological representation of the underlying 3D MOF showing a trinodal 3,4,8-connected net with the unique topology defined by the point symbol of $(4^2.6)_4(4^2.8^4)(4^6.6^4.8^{14}.10^4)$; view along the *a* axis; color codes: centroids of 8-connected $[Co_5(\mu_3\text{-}OH)_2(H_2O)_6]^{8+}$ cluster nodes (magenta balls), centroids of 4-connected $[Co_2(py)_2]^{4+}$ (green balls) and 3-connected btc^{3-} (gray) nodes.

The μ_6-btc^{3-} ligands adopt two different coordination modes (Scheme 1, modes VI and VII), in which the carboxylate groups show the μ_2-η^1:η^1 and μ_2-η^2:η^0 bidentate modes. The dihedral angles between two phenyl rings in the btc^{3-} moieties are 82.58 and 49.02°. The five adjacent Co(II) atoms (a pair of Co1 and Co2 atoms and one Co3 center) are bridged by means of six carboxylate groups from the six different btc^{3-} blocks, two carboxylate O atoms of another two btc^{3-} ligands, and two O atoms of two μ_3-OH$^-$ moieties, giving rise to a centrosymmetric pentanuclear Co(II) subunit (Fig. 6b). In this pentacobalt(II) subunit, the Co···Co distances via μ_3-OH$^-$ linkages vary from 3.090(6) to 3.572(6) Å, and are comparable to those found in other carboxylate and μ_3-OH$^-$-bridged pentacobalt(II) cores.[29] Meanwhile, two crystallographically equal Co4 centers are bridged by four carboxylate groups of four different btc^{3-} ligands, giving rise to a paddle-wheel dinuclear Co$_2$ subunit (Fig. 6c) with a Co···Co separation of 2.813(2) Å. These Co$_5$ and Co$_2$ subunits are multiply interlinked by other COO$^-$ groups of the btc^{3-} blocks to form an intricate 3D metal-organic framework (Fig.

6d), having the shortest distance of 8.709(8) Å between the neighboring Co_5 and Co_2 units. From the topological viewpoint, this 3D MOF features a very complex framework structure composed of the intricate $[Co_5(\mu_3\text{-}OH)_2(H_2O)_6]^{8+}$ subunits (based on Co1, Co2, and Co3 centers), μ_6-btc^{3-} blocks, and the $[Co_2(py)_2]^{4+}$ nodes (based on two Co4 centers). By reducing all these units to centroids, an underlying trinodal 3,4,8-coonected net can be generated (Fig. 6e). It features an unprecedented topology[22] defined by the point symbol of $(4^2.6)_4(4^2.8^4)(4^6.6^4.8^{14}.10^4)$, wherein the $(4^2.6)$, $(4^2.8^4)$, and $(4^6.6^4.8^{14}.10^4)$ indices correspond to the 3-connected btc^{3-}, 4-connected $[Co_2(py)_2]^{4+}$, and 8-connected $[Co_5(\mu_3\text{-}OH)_2(H_2O)_6]^{8+}$ nodes, respectively.

Crystal structure of 9. Compound **9** crystallizes in the monoclinic space group $P2_1/n$ and demonstrates an extremely complex 3D metal-organic framework. In the asymmetric unit, there are three crystallographically unique Pb(II) atoms, two μ_6-btc^{3-} ligands, and one coordinated and one lattice water molecule. As depicted in Fig. 7a, three Pb centers take three different coordination environments. The Pb1 center is coordinated by six carboxylate O atoms from four individual μ_6-btc^{3-} blocks, forming a distorted octahedral $\{PbO_6\}$ geometry. The five-coordinate Pb2 atom adopts a distorted trigonal bipyramidal $\{PbO_5\}$ geometry filled by four carboxylate oxygen atoms from four different μ_6-btc^{3-} ligands and one oxygen atom of H_2O ligand. The Pb3 center is bound by five carboxylate O atoms from the four different μ_6-btc^{3-} ligands, constructing a very distorted square pyramidal $\{PbO_5\}$ geometry. The Pb–O distances range from 2.319(5) to 2.863(5) Å (Table S1, ESI†), being comparable to those found in some reported Pb(II) compounds.[4c,8b,19] In **9**, the btc^{3-} ligands exhibit two different μ_6-coordination modes (Scheme 1, modes VIII and IX), in which the carboxylate groups are the $\eta^1{:}\eta^0$ monodentate, $\eta^1{:}\eta^1$ and μ_2-$\eta^1{:}\eta^1$ bidentate, μ_2-$\eta^2{:}\eta^1$ and μ_3-$\eta^2{:}\eta^1$ tridentate, and μ_3-$\eta^2{:}\eta^2$ tetradentate. The dihedral angles of 43.98 and 36.88° are observed between the two phenyl rings in the μ_6-btc^{3-} blocks. The carboxylate groups of the btc^{3-} ligands multiply bridge the adjacent Pb(II) atoms to form, if seen along the *bc* plane, the 1D double chain motifs (Fig. 7b). These are further assembled into a very complex 3D open framework by additional linkage of btc^{3-} ligands with Pb(II) atoms (Fig. 7c). This framework features channels [7.77 × 6.12 Å measured by atom-to-atom distances], which are filled with guest water molecules of crystallization. Upon their removal, we computed by the PLATON an effective free volume that is 3.5% of the crystal volume.[25] However, after eliminating both coordinated and guest water molecules, the effective free volume attains 6.2% of the crystal volume of **9**. For the sake of topological analysis, the 3D MOF was simplified by reducing μ_6-btc^{3-} blocks to the respective centroids and omitting terminal H_2O ligand. The resulting underlying net (Fig. 7d) is composed of the different 4-connected Pb(II) nodes and two different μ_6-btc^{3-} nodes and can be described as a tetranodal 4,4,6,6-connected framework with the unique topology. It is defined by the point symbol of $(4^2.6^3.8)(4^5.6)_2(4^7.6^6.8^2)(4^8.6^6.8)$.

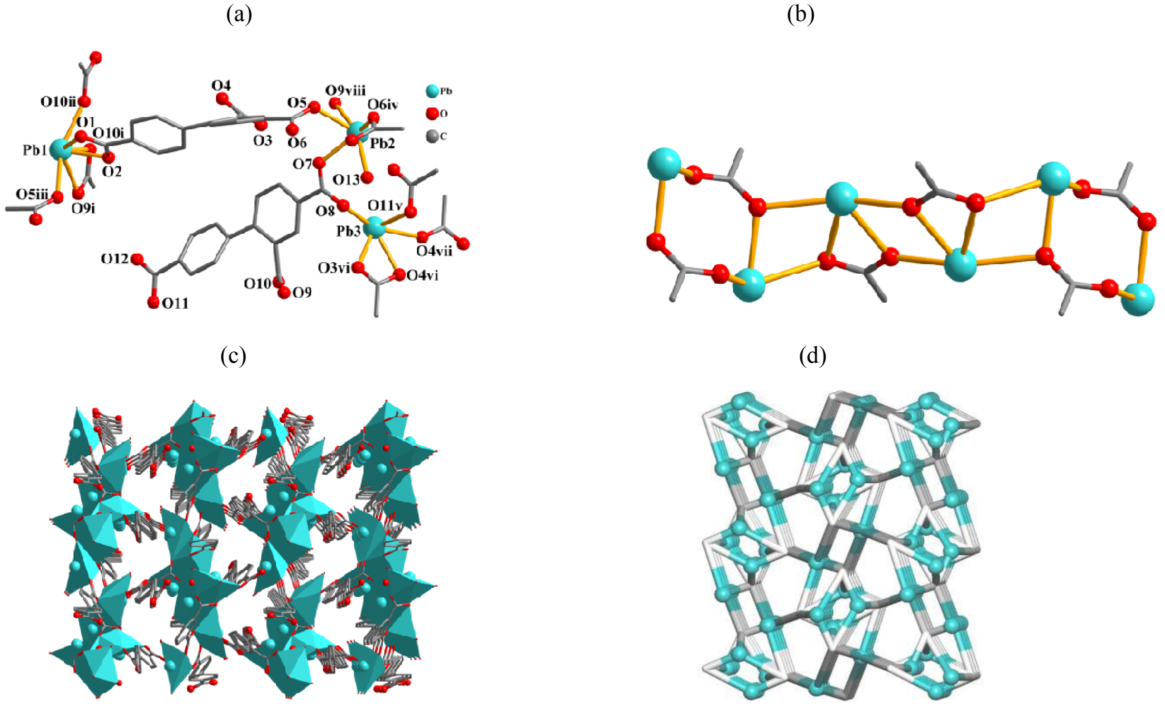

Fig. 7 Structural fragments of **9**. (a) Coordination environment of the Pb(II) atoms. Symmetry codes: i = $-x-1/2, y-1/2, -z+3/2$; ii = $x-1/2, -y+3/2, z-1/2$; iii = $x-1, y, z$; iv = $-x+1, -y+2, -z+1$; v = $x+1, y, z$; vi = $-x+1/2, y+1/2, -z+3/2$; vii = $x+1/2, -y+3/2, z+1/2$; viii = $-x+1/2, y-1/2, -z+3/2$; ix = $-x-1/2, y+1/2, -z+3/2$. (b) 1D double chain motif along the *a* axis. (c) A perspective of 3D metal-organic framework along the *bc* plane. (d) Topological representation of the underlying 3D MOF showing a tetranodal 4,4,6,6-connected net with the unique topology defined by the point symbol of $(4^2.6^3.8)(4^5.6)_2(4^7.6^6.8^2)(4^8.6^6.8)$; view along the *a* axis; color codes: 4-connected Pb nodes (turquoise balls), centroids of 6-connected btc^{3-} nodes (gray).

Coordination modes of H_2btc^{-}/$Hbtc^{2-}$/btc^{3-} blocks and structural comparison

The ligands derived upon deprotonation of biphenyl-2,4,4′-tricarboxylic acid (H_3btc) exhibit nine different coordination modes in compounds **1**–**9** (Scheme 1). Depending on the molar ratio of NaOH and H_3btc during the self-assembly synthesis, the tricarboxylate moiety can adopt partially and fully deprotonated forms such as H_2btc^{-}, $Hbtc^{2-}$, and btc^{3-}. For example, the molar ratios of NaOH and H_3btc of 1:1 and 2:1 led to the H_2btc^{-} and $Hbtc^{2-}$ forms in **1**–**4**. A higher excess of base (molar ratio of NaOH and H_3btc of 3:1) resulted in a completely deprotonated btc^{3-} form in **5** and **9**. It is known that pyridine can be applied not only as an ancillary ligand to facilitate the crystallization of coordination polymers, but also as a deprotonating agent due to its basicity.[30] Given these facts, we have used pyridine instead of NaOH for the self-assembly synthesis of **6**–**8**. The carboxylate groups of biphenyl-2,4,4′-tricarboxylate ligands adopt seven typical modes, including $\eta^1{:}\eta^0$ monodentate, $\eta^1{:}\eta^1$, μ_2-$\eta^2{:}\eta^0$ and μ_2-$\eta^1{:}\eta^1$ bidentate, μ_2-$\eta^2{:}\eta^1$ and μ_3-$\eta^2{:}\eta^1$ tridentate, and μ_3-$\eta^2{:}\eta^2$ tetradentate modes. Besides, an important feature of flexible biphenyl-2,4,4′-tricarboxylate blocks consists in the possibility of the C–C single bond rotation between two aromatic rings (dihedral angles are in the 36.88–82.58° range), thus facilitating the generation of a certain coordination environment around metal ions during the self-assembly process. As a result, the ligands derived from H_3btc can adopt various coordination modes and behave as either terminal (in **1**–**4**) or different μ_4- (in **5**, **6**, and **8**) and μ_6-building blocks (in **7** and **9**). Products **7** and **8** were synthesized under the same reaction conditions, except for a slight difference between the molar ratios of $CoCl_2{\cdot}6H_2O$ and H_3btc (1.5:1 for **7** and 1.77:1 for **8**). The structural differences in these 3D MOFs indicate that the assembly process is also dependent on the molar ratio of metal ion and ligand.

Apart from distinct structural dimensionality of **1**–**9** that ranges from 0D (in **1**–**4**) to 2D (in **5**) and 3D (in **6**–**9**), all the obtained products also reveal a variety of topologies, including their rare or even undocummented types. In fact, the topological classification of the H-bonded or coordination networks disclosed the following underlying nets: **4,5L64** in **1**, **pcu** in **2** and **3**, **sxb** in **4**, **hcb** in **5**, **wei** in **6** and **7**, and topologically unique 3D nets in **8** and **9**.

Thermogravimetric analysis and PXRD results

The thermal stability of compounds **1**–**9** was evaluated under nitrogen atmosphere by thermogravimetric analysis (TGA) and the obtained plots are presented in Fig. 8. The compound **1** loses its one lattice water molecule (exptl, 2.0%; calcd, 1.8%) in the 70–118 °C range, followed by the decomposition at 329 °C. The TGA curves of **2**, **3**, and **5** indicate that these compounds are stable up to 234, 281, and 305 °C, respectively, and then decompose upon further heating. For **4**, there are two distinct thermal effects in the 35–241 °C range that correspond to the removal of two lattice and one coordinated H_2O molecules (exptl, 7.0%; calcd, 7.1%); a dehydrated sample then decomposes at 289 °C. The MOF **6** loses four coordinated water molecules between 29 and 138 °C (exptl, 6.4%; calcd, 6.4%), and then decomposes upon further heating. For metal-organic framework **7**, the weight loss associated with the removal of two crystallization pyridine molecules is observed in the 28–120 °C interval (exptl, 12.0%; calcd, 12.2%), and then decomposes upon further heating. Compound **8** shows the loss of one lattice and three coordinated water molecules between 18 and 85 °C (exptl, 7.2%; calcd, 7.1%), followed by the decomposition of organic ligands. For MOF **9**, there is one distinct thermal effect in the 119–224 °C range that corresponds to the removal of one lattice and one coordinated H_2O molecule (exptl, 2.9%; calcd, 2.9%); further heating up to 368 °C leads to the decomposition of a dehydrated sample.

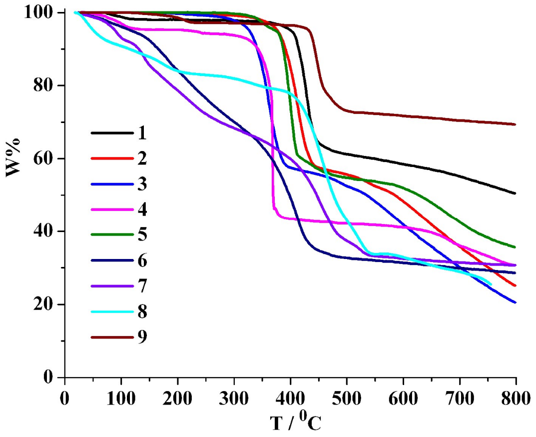

Fig. 8 Thermogravimetric analysis (TGA) curves of compounds **1**–**9**.

The powder X-ray diffraction (PXRD) experiments were carried out for the as-synthesized bulk materials **1**–**9**, showing that the experimental PXRD patterns closely match the simulated ones from the single-crystal X-ray data, thus confirming the purity of samples (Fig. S2, ESI†).

Luminescent Properties

The emission spectra of H_3btc and compounds **1**, **3**, **5** and **9** were measured in the solid-state at room temperature, as depicted in Fig. 9. The "free" H_3btc ligand displays a weak photoluminescence with an emission maximum at 362 nm if excited at 324 nm. For compounds **1**, **3**, **5**, and **9**, the significantly more intense emission bands are observed with the maximum at 388 nm for **1**, 450 nm for **3**, 396 nm for **5**, and 542 nm for **9**, with λ_{ex} of 350 nm in all cases. All bands can be assigned to an intraligand ($\pi^* \rightarrow n$ or $\pi^* \rightarrow \pi$) emission.[20] The enhancement of luminescence of the four compounds can be attributed to the binding of ligands to the metal centers, which effectively increases the rigidity of the ligand and reduces the loss of energy by radiationless decay.[21] It is noteworthy to mention that the compounds **5** and **9** exhibit stronger emission intensities than those of **1** and **3**, what can potentially be explained by their structural differences. In **1** and **3**, the H_2btc^{-} blocks act as simple terminal ligands, while in **5** and **9** the btc^{3-} moieties feature intricate μ_4- and μ_6-coordination fashions, respectively. The later make the ligands more rigid, thus reducing the vibration-induced deactivation.[31,32] The observed photoluminescence of **5** and **9** indicates that these compounds can be excellent candidates for potential applications as photoactive materials.

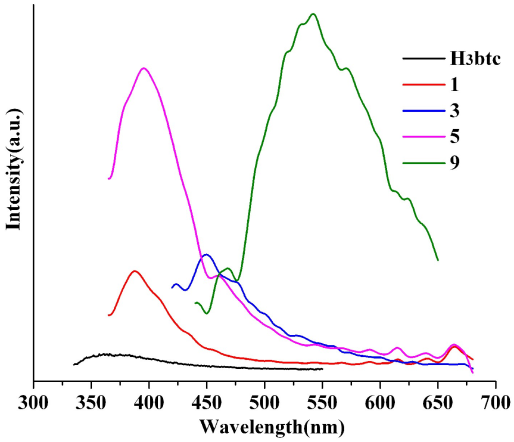

Fig. 9 Solid state emission spectra of H_3btc, **1**, **3**, **5**, and **9** [λ_{ex} was 350 nm].

Magnetic properties

Variable-temperature magnetic susceptibility studies were carried out on powder samples of **6–8** in the 2–300 K temperature range. For the Ni(II) MOF **6**, the $\chi_M T$ value at 300 K is 3.40 $cm^3 \cdot mol^{-1} \cdot K$, which is close to the spin only value of 3.00 $cm^3 \cdot mol^{-1} \cdot K$ for three magnetically isolated Ni(II) centers (S_{Ni} = 1, g = 2.0). Upon cooling, the $\chi_M T$ value drops down very slowly from 3.40 $cm^3 \cdot mol^{-1} \cdot K$ at 300 K to 3.00 $cm^3 \cdot mol^{-1} \cdot K$ at 78 K, and then decreases steeply to 1.15 $cm^3 \cdot mol^{-1} \cdot K$ at 2 K (Fig. 10). In the 11–300 K interval, the χ_M^{-1} *vs.* T plot for **6** obeys the Curie-Weiss law with a Weiss constant θ of –20.53 K and a Curie constant C of 3.60 $cm^3 \cdot mol^{-1} \cdot K$. Because of the long separation between the adjacent Ni_3 subunits, the negative value of θ and the decrease of the $\chi_M T$ should be attributed to the overall antiferromagnetic coupling between the Ni(II) ions within the Ni_3 subunit.

We tried to fit the magnetic data of **6** using the following

$$\chi_M = \frac{N_A g^2 \mu_B^2}{9kT} \frac{3+42\exp(4x)+18\exp(-2x)+15\exp(2x)+3\exp(-6x)}{3+7\exp(4x)+8\exp(-2x)+3\exp(-6x)+\exp(-4x)}$$

expression[33,34] for a trinickel unit:

$$H = -J_{12}\cdot(S_1 \times S_2) - J_{23}\cdot(S_2 \times S_3) - J_{13}\cdot(S_1 \times S_3)$$

where $\chi = J/kT$, $J_{12} = J_{23} = J$, $J_{13} = 0$ (J_{12} and J_{23} are the exchange interactions between the "central" Ni(II) and two "outer" Ni(II) atoms; J_{13} is the exchange interaction between the "outer" Ni(II) ions within a Ni_3 core). Using this model, the susceptibilities for **6** above 12.0 K were simulated, leading to $J = -18.7(5)\ cm^{-1}$ and $g = 2.12$ with the agreement factor R = 6.75×10^{-4} ($R = \Sigma(\chi_{obs}T - \chi_{calc}T)^2 / \Sigma(\chi_{obs}T)^2$). The negative J parameter confirms an antiferromagnetic exchange coupling between the adjacent Ni(II) centers, which is in agreement with a negative θ value. According to the structure of compound **6**, there are two sets of magnetic exchange pathways within the trinickel(II) core, namely via the μ_2-H_2O and μ_2-η^1:η^1-carboxylate (*syn-syn*) bridges (Fig. 5b), which can be responsible for the observed antiferromagnetic exchange.

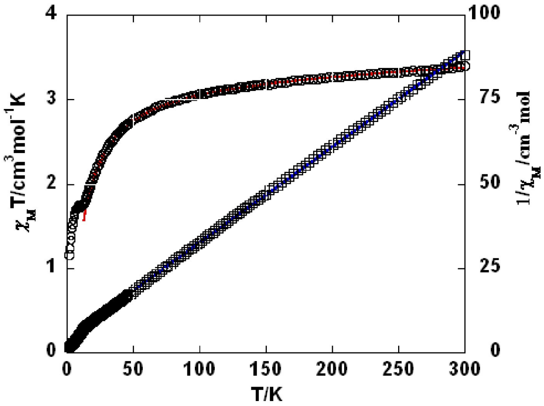

Fig. 10 Temperature dependence of $\chi_M T$ (O) and $1/\chi_M$(□) vs. T for compound **6**. The red line represents the best fit to the equations in the text. The blue line shows the Curie-Weiss fitting.

For MOF **7**, the $\chi_M T$ value of 9.46 $cm^3 \cdot mol^{-1} \cdot K$ at 300 K is much larger than the value (5.61 $cm^3 \cdot mol^{-1} \cdot K$) expected for the two magnetically isolated high-spin Co(II) ions (S = 3/2, g = 2.0). This is a common phenomenon for Co(II) ions due to their strong spin-orbit coupling interactions.[11,29] Upon cooling, $\chi_M T$ decreases gradually and reaches a minimum of 7.21 $cm^3 \cdot mol^{-1} \cdot K$ at 59.9 K. Below 59.9 K, however, the $\chi_M T$ value increases sharply to a maximum of 31.34 $cm^3 \cdot mol^{-1} \cdot K$ at 27.9 K, and then drops to 3.85 $cm^3 \cdot mol^{-1} \cdot K$ at 2 K (Fig. 11). Between 75.9 and 300 K, the magnetic susceptibilities can be fitted to the Curie-Weiss law with C = 9.03 $cm^3 \cdot mol^{-1} \cdot K$ and θ = +8.86 K. The positive θ value indicates the presence of dominant ferromagnetic interactions between the Co(II) ions within the Co_3 subunit. As in the case of **6**, there are also two sets of magnetic exchange pathways within the tricobalt(II) core of **7**, namely via the μ_2-H_2O and μ_2-η^1:η^1-carboxylate (*syn-syn*) bridges. These pathways can be responsible for the observed ferromagnetic exchange.

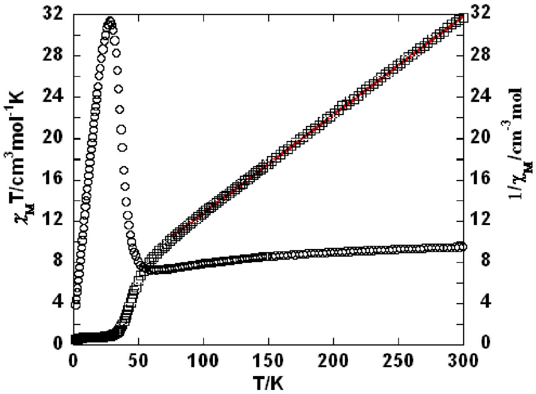

Fig. 11 Temperature dependence of $\chi_M T$ (O) and $1/\chi_M$(□) vs. T for compound **7**. The red line shows the Curie-Weiss fitting.

The temperature-dependent magnetic properties of MOF **8** are shown in Fig. 12 in the form of $\chi_M T$ *vs.* T curve. The $\chi_M T$ value of 13.94 $cm^3 \cdot mol^{-1} \cdot K$ at 300 K is much larger than the value (6.54 $cm^3 \cdot mol^{-1} \cdot K$) expected for three and a half magnetically isolated high-spin Co(II) ions (S = 3/2, g = 2.0). Upon lowering the temperature, the χ_MT parameter rapidly decreases to a minimum value of 8.43 $cm^3 \cdot mol^{-1} \cdot K$ at 57.9 K, and then abruptly increases to a sharp maximum (13.94 $cm^3 \cdot mol^{-1} \cdot K$) at 2.9 K, and then finally decreases on further cooling. Between 200 and 300 K, the magnetic susceptibilities can be fitted to the Curie-Weiss law with $C = 13.6$ cm^3 mol^{-1} K and $\theta = -2.1$ K. The negative θ value clearly indicates an antiferromagnetic exchange between the adjacent Co(II) centers. Because of the long separation between the adjacent Co_2 and Co_5 subunits, the negative value of θ should be attributed to the overall antiferromagnetic coupling between the Co(II) atoms within the Co_2 and Co_5 cores. According to the crystal structure of **8** (Fig. 6), there are two sets of magnetic exchange pathways within the Co_5 subunit (one is through carboxylate bridges and the other one is via μ_3-OH^- bridges), whereas the Co_2 subunit shows only carboxylate bridges.

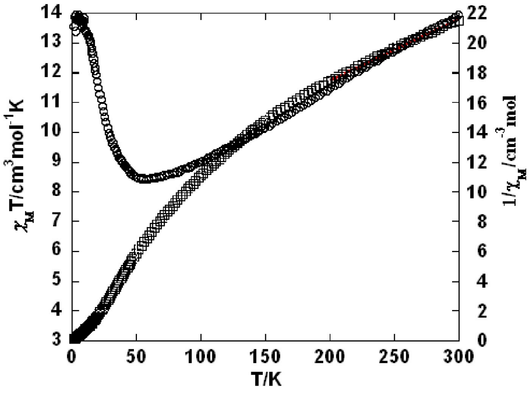

Fig. 12 Temperature dependence of $\chi_M T$ (O) and $1/\chi_M$(□) vs. T for compound **8**. The red line shows the Curie-Weiss fitting.

Conclusions

The current study has shown that biphenyl-2,4,4'-tricarboxylic acid can act as a versatile main building block toward the generation, by a hydrothermal self-assembly pathway, of a series of novel metal(II) (Zn, Ni, Co, Cd, and Pb) coordination compounds. Hence, by selecting different metal(II) nodes and adjusting the molar ratio between metal ion, H_3btc block, NaOH, and/or the type of the aromatic *N*-donor ancillary ligand, we have assembed a diversity of new compounds using water as reaction medium. The obtained structures vary from the intricate 3D metal-organic frameworks **6**–**9** to 2D coordination polymer **5** and discrete 0D monomers **1**–**4**. The structures of **1**–**5** are further extended [0D→3D (**1**–**4**) and 2D→3D (**5**)] into various H-bonded networks by means of conventional hydrogen bonds. Besides, product **1** is the first Zn(II) containing coordination compound derived from H_3btc, whereas complexes **1**–**4** represent the first compounds with the H_2btc^- or $Hbtc^{2-}$ moieties acting as terminal ligands. The generated products **1**–**9** not only represent distinct dimensionality but also reveal a high diversity of topological types. In fact, some topologically unique multinodal nets have been found in the very complex 3D metal-organic frameworks of Co(II) and Pb(II) contaning products, thus providing a contribution toward the identification of new topological types in crystal engineering research. Further exploration of biphenyl-2,4,4'-tricarboxylic acid and derived flexible building blocks toward the construction of functional metal-organic networks is currently in progress.

Acknowledgements

This work was financially supported by the National Natural Science Foundation of China (Project 21201091). AMK acknowledges the Foundation for Science and Technology (FCT), Portugal (PTDC/QUI-QUI/121526/2010, PEst-OE/QUI/UI0100/2013).

Notes and references

[a] Key Laboratory of Nonferrous Metal Chemistry and Resources Utilization of Gansu Province and College of Chemistry and Chemical Engineering
Lanzhou University, Lanzhou, 730000 (P. R. China)
Fax: +86-931-89151962; Tel: +86-931-8915196;
[b] Centro de Química Estrutural, Complexo I, Instituto Superior Técnico, Universidade de Lisboa, Av. Rovisco Pais, 1049-001, Lisbon (Portugal)
E-mail: gujzh@lzu.edu.cn;ywwang@lzu.edu.cn

†Electronic Supplementary Information (ESI) available: tables containing selected bond distances and angles and hydrogen bonding parameters, additional structural representation and PXRD patterns of ***1**–**9**; crystallographic data in CIF format.*

1 (*a*) M. H. Liu, L. Zhang and T. Y. Wang, *Chem. Rev.*, 2015, **115**, 7304; (*b*) M. Dinca and J. R. Long, *J. Am. Chem. Soc.*, 2005, **127**, 9376; (*c*) W. X. Zhang, P. Q. Liao, R. B. Lin, Y. S. Wei, M. H. Zeng and X. M. Chen, *Coord. Chem. Rev.*, 2015, **293**, 263; (*d*) Q. L. Zhu and O. Xu, *Chem. Soc. Rev.*, 2014, **43**, 5468; (*e*) X. D. Zheng and T. B. Lu, *CrystEngComm*, 2010, **12**, 324; (*f*) G. Férey, *Chem. Soc. Rev.*, 2008, **37**, 191; (*g*) Z. Q. Wang and S. M. Cohen, *Chem. Soc. Rev.*, 2009, **38**, 1315; (*h*) J. R. Li, R. J. Kuppler, H. C. Zhou, *Chem. Soc. Rev.*, 2009, **38**, 1477; (*i*) G. Ferey and C. Serre, *Chem. Soc. Rev.*, 2009, **38**, 1380; (*j*) Q. W. Li, W. Y. Zhang, O. S. Miljanic, C. H. Sue, Y. L. Zhao, L. H. Li, C. B. Knobler, J. Fraser Stoddart and O. M. Yaghi, *Science*, 2009, **325**, 855; (*k*) Y. Ma, A. L. Cheng, B. Tang and E. Q. Gao, *Dalton Trans.*, 2014, **43**, 13957; (*l*) B. Xu, J. Li, N. N. Kong and C. C. Li, *Inorg. Chem. Commun.*, 2014, **47**, 119; (*m*) G. M. Zhuang, X. B. Li and E. Q. Gao, *Inorg. Chem. Commun.*, 2014, **47**, 134.

2 (*a*) X. F. Zheng and L. G. Zhu, *J. Mol. Struct.*, 2013, **1039**, 1; (*b*) J. Z. Gu, D. Y. Lv, Z. Q. Gao, J. Z. Liu and W. Dou, *Transition Met. Chem.*, 2011, **36**, 53.

3 (*a*) L. Y. Yang, L. L. Xin, W. Gu, J. L. Tian, S. Y. Liao, P. Y. Du, Y. Z. Tong, Y. P. Zhang, R. Lv, J. Y. Wang and X. Liu, *J. Solid State Chem.*, 2014, **218**, 64; (*b*) Y. X. Hu, Y. T. Qian, W. W. Zhang, Y. Z. Li and J. F. Bai, *Inorg. Chem. Commun.*, 2014, **47**, 102; (*c*) B. Van de Voorde, B. Bueken, J. Denayer and D. D. Vos, *Chem. Soc. Rev.*, 2014, **43**, 5766; (*d*) S. Y. Yang, H. B. Yuan, X. B. Xu and R. B. Huang, *Inorg. Chim. Acta*, 2013, **403**, 53.

4 (*a*) S. Ganguly and R. Mondal, *Cryst. Growth Des.*, 2015, **15**, 2211; (*b*) G. Akiyama, R. Matsuda, H. Sato and S. Kitagawa, *Chem. Asi. J.*, 2014, **9**, 2772; (*c*) L. Hashemi, A. Morsali, V. T. Yilmaz, O. Büyükgüngor, H. R. Khavasi, F. Ashouri and M. Bagherzadeh, *J. Mol. Struct.*, 2014, **1072**, 260; (*d*) J. Gas, A. Corma, F. Kapteijn and F. X. L. Xamena, *ACS Catal.*, 2014, **4**, 361.

5 (*a*) H. Erer, O. Zafer and M. Arıcı, *Cryst. Growth Des.*, 2015, **15**, 3201; (*b*) Y. P. He, Y. X. Tan and J. Zhang, *Inorg. Chem.*, 2013, **52**, 12758; (*c*) X. Y. Duan, Q. Q. Meng, Y. Su, Y. Z. Li, C. Y. Duan, X. M. Ren and C. S. Lu, *Chem. Eur. J.*, 2011, **17**, 9936.

6 (*a*) C. D. Si, D. C. Hu, Y. Fan, Y. Wu, X. Q. Yao, Y. X. Yang and J. C. Liu, *Cryst. Growth Des*., 2015, **15**, 2419; (*b*) H. Wang, X. Y. Yang, Y. Q. Ma, W. B. Cui, Y. H. Li, W. G. Tian, S. Yao, Y. Gao, S. Dang and W. Zhu, *Inorg. Chim. Acta*., 2014, **416**, 63; (*c*). F. A. L. Porta, P. H. Ramos, E. C. d Resende, M. C. Guerreiro, J. O. S. Giacoppo, T. C. Ramalho, J. R. Sambrano, J. Andrés and E. Longo, *Inorg. Chim. Acta*, 2014, **416**, 200; (d) W. G. Lu, L. Jiang, X. L. Feng and T. B. Lu, *Inorg. Chem*., 2009, **48**, 6997.

7 (*a*) S. S. Y. Chui, S. M. F. Lo, J. P. H. Charmant, A. G. Orphen and I. D. Willians, *Science*, 1999**, 283**, 1148; (*b*) S. Horike, R. Matsuda, D. Tanaka, M. Mizuno, K. Endo and S. Kitagawa, *J. Am. Chem. Soc*., 2006, **128**, 4222; (*c*) J. Z. Gu, W. G. Lu, L. Jiang, H. C. Zhou and T. B. Lu, *Inorg. Chem*., 2007, **46**, 5835; (*d*) F. Condello, F. Garau, A. Lanza, M. Monari, F. Nestola, L. Pandolfo and C. Pettinari, *Cryst. Growth Des*., 2015, **15**, 4854; (*e*) X. L. Luo, L. B. Sun, J. Zhao, D. S. Li, D. M. Wang, G. H. Li, Q. S. Huo and Y. L. Liu, *Cryst. Growth Des*., 2015, **15**, 4901.

8 (*a*) J. Z. Gu, Z. Q. Gao and Y. Tang, *Cryst. Growth Des*., 2012, **12**, 3312; (*b*) J. Z. Gu, A. M. Kirillov, J. Wu, D. Y. Lv, Y. Tang and J. C. Wu, *CrystEngComm*, 2013, **15**, 10287; (*c*) Z. Q. Gao, H. J. Li and J. Z. Gu, *Chin. J. Inorg. Chem.* 2014, **30**, 1421. (*d*) B. L. Chen, N. W. Ockwig, A. R. Millward, D. S. Contreras and O. M. Yaghi, *Angew. Chem., Int. Ed*., 2005, **44**, 4745.

9 (*a*) D. Tian, Y. Pang, Y. H. Zhou, L. Guan and H. Zhang, *CrystEngComm*, 2011, **13**, 957; (*b*) L. L. Wen, F. Wang, X. K. Leng, C. G. Wang, L. Y. Wang, J. M. Gong and D. F. Li, *Cryst. Growth Des*., 2010, **10**, 2835.

10 (*a*) Y. Zhao, X.H. Chang, G.Z. Liu, L.F. Ma, L.Y. Wang, *Cryst. Growth Des*., 2015, **15**, 966; (*b*) J. W. Wang, Y. C. Su and J. J. Wang, *Chinese J. Struct. Chem*., 2015, **34**, 1385.

11 D. Y. Wang, H. H. Zou, F. L. Hu and Y. J. Li, *Inorg. Chem. Commun*., 2012, **26**, 1.

12 (*a*) X. Y. Wan, F. L. Jiang, L. Chen, M. Y. Wu, M. J. Zhang, J. Pan, K. Z. Su, Y. Yang and M. C. Hong, *Cryst. Growth Des*., 2015, **15**, 1481; (*b*) L. N. Zhang, C. Zhang, B. Zhang, C. X. Du and H. W. Hou, *CrystEngComm*, 2015, **17**, 2837; (*c*) X. X. Xu, Y. Lu, E. B. Wang, Y. Ma and X. L. Bai, *Cryst. Growth Des*., 2006, **6**, 2029; (*d*) M. Du, C. P. Li, C. S. Liu and S. M. Fang, *Coord. Chem. Rev*., 2013, **257**, 1282.

13 (*a*) C. Y. Niu, X. F. Zheng, X. S. Wan and H. Z. Kou, *Cryst. Growth Des*., 2011, **11**, 2874; (*b*) K. H. Li, W. C. Song, Y. W. Li, Y. Q. Chen and X. H. Bu, *Cryst. Growth Des*., 2012, **12**, 1064; (*c*) M. Chen, S. S. Chen, T. Okamura, Z. Su, M. S. Chen, Y. Zhao and W. Y. Sun, *Cryst. Growth Des*., 2011, **11**, 1901.

14 (*a*) X. M. Chen and M. L. Tong, *Acc. Chem. Res*., 2007, **40**, 162; (*b*) R. Singh and P. K. Bharatdwaj, *Cryst. Growth Des*., 2013, **13**, 3722; (*c*) A. M. Stepenson, D. Ward, *Chem. Commun*, 2012, **48**, 3605.

15 L. V. Tsymbal, I. L. Andriichuk, Ya. D. Lampeka and V. B. Arion, *J. Struct. Chem*., 2014, **55**, 1466.

16 H. J. Li, Z. Q. Gao and J. Z. Gu, *Chin. J. Inorg. Chem*., 2014, **30**, 2615.

17 B. B. Ding, Y. Q. Weng, Z. W. Mao, C. K. Lan, X. M. Chen and B. H. Ye, *Inorg. Chem*., 2005, **44**, 8836.

18 (*a*) L.Chen, S. H. Gou and J. Q. Wang, *J. Mol. Struct*., 2011, **991**, 149; (*b*) W. L. Liu, L. H. Ye, X. F. Liu, L. M. Yuan, J. X. Jiang, C. G. Yan, *CrystEngComm*, 2008, **10**, 1395.

19 J. Z. Gu, Y. H. Cui, J. Wu and A. M. Kirillov, *RSC Adv*., 2015, **5**, 78889.

20 J. Z. Gu, D. Y. Lv, Z. Q. Gao, J. Z. Liu, W. Dou and Y. Tang, *J. Solid State Chem*., 2011, **184**, 675.

21 (*a*) G. M. Sheldrick, *Acta Crystallogr., Sect. A: Found. Crystallogr*., 1990, **46**, 467; (*b*) G. M. Sheldrick, *SHELXS-97,* A Program for X-ray Crystal Structure Solution, and *SHELXL-97*, A Program for X-ray Structure Refinement, Göttingen University, Germany, 1997.

22 (*a*) V. A. Blatov, *IUCr CompComm Newsletter*, 2006, **7**, 4; (*b*) V. A. Blatov, A. P. Shevchenko and D. M. Proserpio, *Cryst. Growth Des*., 2014, **14**, 3576.

23 (*a*) X. L. Yang, M. H. Xie, C. Zou, Y. B. He, B. L. Chen, M. O'Keeffe and C. D. Wu, *J. Am. Chem. Soc*., 2012, **134**, 10638; (*b*) T. T. Cao, Y. Q. Peng, T. Liu, S. N. Wang, J. M. Dou, Y. W. Li, C. H. Zhou, D. C. Li and J. F. Bai, *CrystEngComm*, 2014, **16**, 10658.

24 (*a*) J. Yang, G. B. Che, B. Liu, Y. Y. Liu and J. F. Ma, *Inorg. Chem. Commun*., 2010, **13**, 112; (*b*) S. I. Noro, T. Akutagawa and T. Nakamura, *Cryst. Growth Des*., 2007, **7**, 1205; (*c*) G. D. Yang, J. C. Dai, Y. X. Lian, W. S. Wu, J. M. Li, S. M. Hu, T. L. Sheng, Z. Y. Fu and X. T. Wu, *Inorg. Chem*., 2007, **46**, 7910.

25 P. Van der Sluis and A. L. Spek, *Acta Crystallogr., Sect. A: Found. Crystallogr*., 1990, **46**, 194.

26 (*a*) M. O'Keeffe and O. M. Yaghi, *Chem. Rev*., 2012, **112**, 675; (*b*) M. Li, D. Li, M. O'Keeffe and O. M. Yaghi, *Chem. Rev*., 2014, **114**, 1343.

27 The Reticular Chemistry Structure Resource (RCSR) Database; M. O'Keeffe, M. A. Peskov, S. J. Ramsden and O. M. Yaghi, *Acc. Chem. Res*., 2008, **30**, 1782.

28 See the Cambridge Structural Database (CSD, version 5.36, 2015): F. H. Allen, *Acta Crystallogr.*, 2002, **B58**, 380.

29 (*a*) L. L. Wen, Z. D. Lu, X. M. Ren, C. Y. Duan, Q. J. Meng and S. Gao, *Cryst. Growth Des*., 2009, **9**, 227; (*b*) R. Kuhlman, G. L. Schimek and J. W. Kolis, *Inorg. Chem*., 1999, **38**, 194; (*c*) B. Y. Li, X. J. Zhou, G. H. Li, J. Hua, Y. Bi, Y. J. Li, Z. Shi and S. H. Feng, *CrystEngComm*, 2011, **13**, 4592; (*d*) S. P. Bew, A. D. Burrows, T. Düren, M. F. Mahon, P. Z. Moghadam, V. M. Sebestyen and S. Thurston, *Chem. Commun*, 2012, **48**, 4824.

30 (*a*) C. E. Sumner, *Inorg. Chem*., 1988, **27**, 1320; (*b*) J. K. Beattle, T. W. Hambley, J. A. Klepetko, A. F. Masters and P. Turner, *Polyhedron*, 1996, **15**, 2141; (*c*) Y. L. Shao, Y. H. Cui, J. Z. Gu, A. M. Kirillov and J. Wu, *RSC Adv*., 2015, **5**, 87484.

31 (*a*) D. Sun, L. L. Han, S. Yuan, Y. K. Deng, M. Z. Xu and D. F. Sun, *Cryst. Growth Des*., 2013, **13**, 377; (*b*) Q. L. Zhu, C. J. Shen, C. H. Tan, T. L. Sheng, S. M. Hua and X. T. Wu, *Chem. Commun*., 2012, **48**, 531; (*c*) Y. J. Cui, Y. F. Yue, G. D. Qian and B. L. Chen, *Chem. Rev*., 2012, **112**, 1126.

32 (*a*) Y. Zhang, B. B. Guo, L. Li, S. F. Liu and G. Li, *Cryst. Growth Des*., 2013, **13**, 367; (*b*) L. Zhang, Z. J. Li, Q. P. Lin, Y. Y. Qin, J. Zhang, P. X. Yin, J. K. Cheng and Y. G. Yao, *Inorg. Chem*., 2009, **48**, 6517; (*c*) Y. Qi, Y. X. Che, F. Luo, S. R. Batten, Y. Liu and J. M. Zheng, *Cryst. Growth Des*., 2008, **8**, 1654.

33 F. J. Rietmeijer, G. A. V. Albada, R. A. G. D. Graaff, J. G. Haasnoot and J. Reedijk, *Inorg. Chem*., 1985, **24**, 3597.

34 A. Banerjee, P. Mahata and S. Natarajan, *Eur. J. Inorg. Chem*., 2008, 3501.

Exploring biphenyl-2,4,4′-tricarboxylic acid as a flexible building block for the hydrothermal self-assembly of diverse metal-organic and supramolecular networks

Yong-Liang Shao, Yan-Hui Cui, Jin-Zhong Gu*, Jiang Wu, Ya-Wen Wang*,

Alexander M. Kirillov

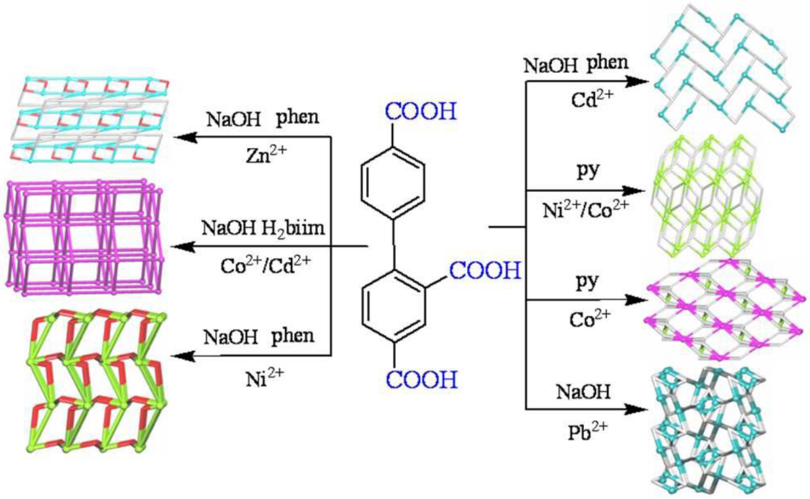

This contribution reports the hydrothermal self-assembly synthesis, characterization, thermal stability, structural and topological features, and luminescent or magnetic properties of a new series of nine coordination compounds, including very complex and topologically unique MOFs.